Halogen-Bond Effects on the Thermo- and Photochromic Behaviour of Anil-Based Molecular Co-crystals

FULL PAPER

Halogen bond effects on the thermo- and photochromic behaviour of anil-based molecular co-crystals

Andrea Carletta,[‡[a]] Floriana Spinelli, [‡ [b]] Simone d'Agostino,[[b]] Barbara Ventura,*[[c]] Michele R. Chierotti,[[d]] Roberto Gobetto[[d],] Johan Wouters,*[[a]] Fabrizia Grepioni*[[b]]

Abstract: N-salicilideneanilines are among the most studied thermochromic and photochromic systems in the solid state. Although thermochromism is a general property of crystalline N-salicilideneanilines, photochromism is known in a limited number of cases. We report here, as a method for the construction of thermo- and photo-responsive molecular architectures, the co-crystallization of 1,2,4,5-tetrafluoro-3,6-diiodobenzene (**I2F4**) with three selected imines of *o*-vanillin, named **1**, **2** and **3**, obtained via condensation reaction with 3-aminopyridine, 4-bromoaniline and 4-iodoaniline, respectively. All crystals and co-crystals have been characterized by means of solid-state complementary techniques (crystallography, solid state NMR, absorption and emission spectroscopy). The role of halogen bonding and crystal packing in the optical and chromic properties of all solid materials is discussed. All solids exhibit thermochromic behavior, and three of them (**2**, $\mathbf{2_2}$·**I2F4** and $\mathbf{3_2}$·**I2F4**) are found to be also photochromic. Imine derivative **3** crystallizes in two different polymorphic forms (**3A** and **3B**) and a solvate ($\mathbf{3_{solv}}$). The bromo- and iodo-derivatives **2** and **3B** are isomorphous and form isomorphous co-crystals with **I2F4**, but behave differently when exposed to UV light, as only crystalline **2** is photochromic**.** Interestingly, replacement of bromine with iodine seems to turn off the photochromism, as also crystalline **3A** and $\mathbf{3_{solv}}$, and even the $\mathbf{2_{0.7}3_{0.3}}$ solid solution, do not manifest photochromic behaviour.

Introduction

Thermo- and photochromism are color change phenomena induced by variation of temperature and by absorption of electromagnetic radiation, respectively.[1] Photo- and thermochromic materials have been attracting increasing interest due to their broad range of applications *e.g*. in information storage, electronic display systems, optical switching devices and sensors.[2,3] Among thermo- and photochromic compounds, N-salicylideneanilines and their derivatives have received particular attention, due to ease of preparation and their ability to switch between three different forms: a colorless enol form, a yellow *cis*-keto form and a red *trans*-keto form.[4] The accepted mechanism for thermochromism is a temperature dependent ground-state keto-enol tautomerization via intramolecular proton transfer between the enol form and the *cis*-keto form.[5] If these two forms are properly irradiated (365 nm for the enol form and 450 nm for the *cis*-keto form), they undergo a *cis-trans* photo-isomerization toward the *trans*-keto form, through the formation of an excited *cis*-keto intermediate, originating from an excited state intramolecular proton transfer (ESIPT) process in case of excitation of the enol tautomer (Scheme 1).[6] Most N-salicylideneanilines (also named anils) exhibit thermochromic behavior in their solids, whereas photochromism is rarely observed in these systems. According to the proposed "pedal-motion" mechanism of *cis-trans* photoisomerization, photochromism should be observed only if the molecule possesses the necessary reaction volume for the isomerization to occur within the crystal.[7] It has been stated that only non-planar anils characterized by dihedral angles Φ > 30° between the aromatic ring planes should exhibit photochromic properties. In contrast, near-planar conformations (Φ < 20°) should promote a close-packed molecular arrangement that would hinder rotational motion in the crystal, resulting in non-photochromic behaviour.[4,8] However, a number of studies has shown the limit of such empirical rule.[9–11] A first method adopted for the obtainment of solid photochromic forms is the introduction of bulky substituents, like *tert*-butyl or trityl groups, that can act as space-openers.[12,13] A promising alternative to the chemical modification approach is represented by *crystal engineering.*[14–19] This second approach has the advantage of allowing modification of the crystal structure by keeping the same chromophore component. To this purpose, co-crystallization and salification have shown to be two effective methods to induce photochromic properties in anil-based systems.[9,11,20] We report co-crystallization of N-salicylidene-aniline/aminopyridine derivatives with a halogenated coformer, 1,2,4,5-tetrafluoro-3,6-diiodobenzene (**I2F4**).[21] The specific advantages derived from the use of the halogen bond[22] in the construction of supramolecular architectures are nowadays demonstrated in materials science (*e.g* supramolecular liquid crystals,[23] supramolecular gelators,[24] fluorescence-enhancement[25] and phosphorescent materials[26,27]) and in drug development.[28] In this light, we have selected three different imines (labeled here **1**,[29] **2**[30] and **3**, see Scheme 2) of 2-hydroxy-3-methoxybenzaldehyde (*i.e ortho*-vanillin) as model compounds for co-crystallization, to assess the role of both crystal packing

[a] Andrea Carletta, Prof. Dr. Johan Wouters
Department of Chemistry, University of Namur (UNamur), Rue de Bruxelles 61, Namur, 5000 (Belgium)
E-mail: johan.wouters@unamur.be
[b] Floriana Spinelli, Dr. Simone d'Agostino, Prof. Dr. Fabrizia Grepioni
Università di Bologna, Dipartimento di Chimica G. Ciamician, Via Selmi 2, 40126 Bologna, Italy
E-mail: fabrizia.grepioni@unibo.it
[c] Dr. Barbara Ventura
Istituto per la Sintesi Organica e la Fotoreattività (ISOF) – CNR, Via P. Gobetti 101, 40129 Bologna, Italy.
E-mail: barbara.ventura@isof.cnr.it
[d] Prof. Dr. Michele R. Chierotti, Prof. Dr. Roberto Gobetto
Dipartimento di Chimica and NIS Centre, Università di Torino, via Giuria 7,10125 Torino, Italy.
‡ Both authors contributed equally to this work

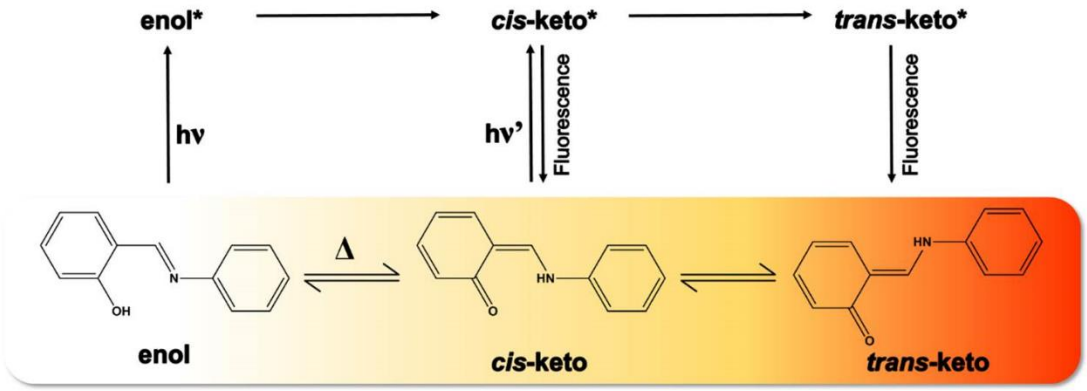

Scheme 1. General pathway of ground and excited state thermo- and photochromic processes in N-salicylideneanilines.

and halogen bonding in tuning the photo- and thermochromic properties of N-salicylideneanilines.

Compound **1** belongs to the family of N-salicylide-3-aminopyridines, whereas compounds **2** and **3** are *p*-halo monosubstituted N-salicylideneanilines. Specifically, in the first case we expect the N-atom of the pyridine moiety of **1** to act as a halogen-bond acceptor for **I2F4** by formation of an $N_{pyridine}$···I synthon in a **1_2·I2F4** co-crystal). In the other two cases (**2_2·I2F4** and **3_2·I2F4** co-crystals), due to the absence of the strong $N_{(pyridine)}$-atom acceptor, the halogen-bond interaction with the coformer is expected to be directed toward the hydroxyl moiety of the chromophore (the tautomerization center), by a $O_{(hydroxyl)}$···I synthon.

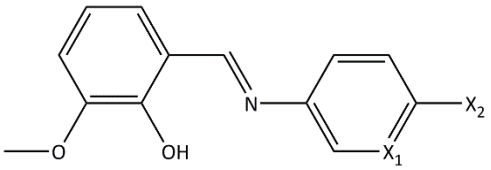

Scheme 2. Molecular diagram for the 2-hydroxy-3-methoxybenzaldehyde derivatives **1** (X_1 = N, X_2 = H), **2** (X_1 = C, X_2 = Br) and **3** (X_1 = C, X_2 = I).

Presence of the para-halogen atom in **2** and **3** potentially allows for halogen···halogen interactions (unsymmetrical I···Br and symmetrical I···I type, for **2** and **3**, respectively).[31] Mechanochemical synthesis is used to prepare the solids of interest.[32,33] All crystalline solids obtained are investigated by means of X-ray single crystal (at room and low temperature) and powder diffraction, solid-state absorption and emission spectroscopy, Fourier-transformed IR spectroscopy and ^{13}C and ^{15}N CPMAS solid-state NMR.

Results and Discussion

Structural characterization

The crystal packing features of parent compounds **1**, **2** and **3** and of the co-crystalline materials obtained by reaction with **I2F4** will be discussed in the following. This is accompanied by an analysis of the **T1** and **T2** torsion angles, defined in Scheme 3a. A **T1** angle close to 0° is associated with the *cis*-form. The **T2** angle in the enol tautomer is usually close to 0°, because the intramolecular hydrogen bond involving the –OH group and the imine nitrogen forces the fragment to be planar. The value of the **Φ** angle between the rings planes, defined in Scheme 3b, will also be considered, and its value related to the solid-state photochromic or non-photochromic behaviour of all the compounds presented in this work.

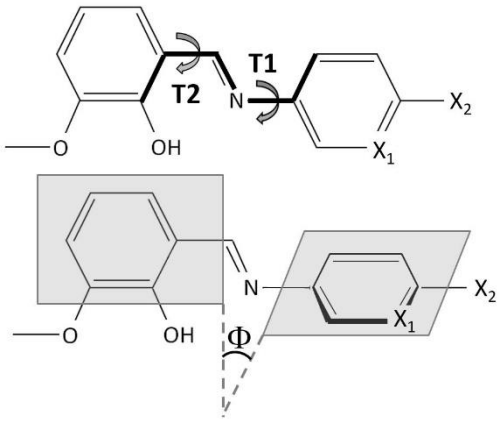

Scheme 3. (a) Definition of the **T1** and **T2** torsion angles in the anil derivatives. (b) The **Φ** dihedral angle formed by the two six-membered rings.

*The starting compounds: **1**, **2** and **3***

Figure 2 . Single crystals of compounds **1** (left), **2** (middle) and **3_{solv}**,(right) obtained by recrystallization from solution of the mechanosynthesis products (see Experimental).

Compound 1. Compound **1** crystallizes in the orthorhombic $P2_12_12_1$ space group. The tautomeric form observed at both room temperature [22] and 108 K is the enol form, as deduced from selected bond lengths (Table 1). The crystal cohesion is mainly due to dispersion forces, as the only strong hydrogen bond is of

the intramolecular type ($S_1^1(6)$): it involves the hydroxyl group and the iminic nitrogen, and constraints the **T2** torsion angle to the near-planar value of 2.0(3)° (see Table 1). The **T1** torsion angle exhibits a value of about -32° in both the RT and the LT determinations. Calculated value of Φ (dihedral angle between aromatic rings) is 31.4° in the RT structure and 31.7° at low temperature. Despite having Φ > 30°, **1** has been reported to present only thermochromic behaviour.[9]

Table 1. Selected geometries: bond distances, torsion angles T1 (see Scheme 3) and dihedral angles Φ between the benzene rings

	N1–C7 (Å)	C6–O1 (Å)	T1 (deg)	T2 (deg)	Φ (deg)
1 (RT)	1.281(3)	1.353(3)	-32.2(3)	1.4(3)	31.4
1 (LT)	1.289(3)	1.357(3)	-32.1(3)	2.0(3)	31.7
2 (RT)	1.281(7)	1.350(6)	12.9(4)	2.8(8)	10.5
2 (LT)	1.291(4)	1.356(3)	12.9(5)	2.4(6)	10.5
3_{solv} (RT)	1.281(7)	1.352(7)	1.1(7)	1.0(8)	2.4
	1.269(6)	1.345(6)	18.1(8)	1.1(8)	20.0
3_{solv} (LT)	1.293(5)	1.359(5)	5.2(5)	1.2(6)	7.8
	1.298(4)	1.364(4)	20.8(5)	0.6(5)	20.4
3A	1.301(11)	1.323(7)	18(1)	2(1)	15.8
3B	1.263(12)	1.352(10)	16(1)	4(2)	14.3
$2_{0.7}3_{0.3}$	1.310(13)	1.358(11)	18(2)	3(2)	13.4
1_2·I2F4 (RT)	1.282(6)	1.342(4)	153.6(4)	0.8(6)	34.3
1_2·I2F4 (LT)	1.297(9)	1.357(9)	153.6(7)	0(1)	34.8
2_2·I2F4 (RT)	1.268(6)	1.362(6)	36.1(7)	1.9(7)	34.4
2_2·I2F4 (LT)	1.290(5)	1.363(4)	35.4(5)	2.0(5)	33.0
3_2·I2F4 (RT)	1.272(6)	1.358(5)	34.2(6)	2.6(7)	31.3
3_2·I2F4 (RT)	1.291(4)	1.357(4)	31.3(4)	2.0(4)	29.3

Compound 2. Compound **2** crystallizes in the orthorhombic $P2_12_12_1$ space group. As in the case of **1**, the only tautomeric form detected at the experimental conditions (both RT and 147 K) is the enol form. The hydroxyl group on one side, and the iminic nitrogen on the other side, force the **T2** torsion angle to a near-planar value, whereas **T1** and Φ are 12.9° and 10.5°, respectively (see Table 1). No important variations on bond length and torsion angles are found by comparison between LT and RT crystallographic determinations. The crystal packing is dominated by π-stacking, with piles of molecules arranged in a zig-zag fashion, as shown in Figure 2. Compound **2** is reported to present only solid-state thermochromism.[34]

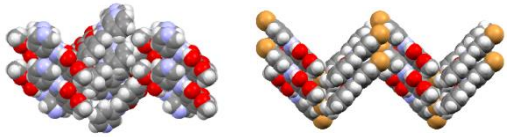

Figure 3. *Crystal packing in solid **1**(left) and **2** (right).*

Compound 3. The substitution of bromine for iodine results in a tendency to form multiple crystal forms (see Figure 3).

Firstly, orange-red blocks ($P2_1/c$) were obtained by slow evaporation from a saturated solution in EtOH (form **3A**). Molecules of **3** in structure **3A** are affected by positional disorder around a *pseudo* mirror plane perpendicular to the molecular plane (see Experimental). Near-planar molecules (T1 ca. 2 deg.) are stacked along the *c*-axis and then arranged in a zig-zag fashion by a synergy of C–I···I (halogen···halogen interactions of type II) and C-H···π contacts (see Figure 3).

Secondly, recrystallization in toluene yielded orange-red prisms. This second crystal form, labeled **3B** ($P2_12_12_1$ space group), is isomorphous with **2** (see Figure 3)**.**

Lastly, large orange-red prisms were formed via slow evaporation of an EtOAc solution (form $\mathbf{3_{solv}}$). These latter belong to the triclinic $P\bar{1}$ space group, with two molecules in the asymmetric unit. Within the $\mathbf{3_{solv}}$ structure, pairs of molecules interact by π-π stacking in a head-to-tail fashion. Pairs are arranged over a layer in a herringbone pattern, in which molecules are held together by C–I···π contacts. Crystalline $\mathbf{3_{solv}}$ is, however, characterized by the presence of large voids in its structure (see Figure 3), which could provide the necessary degree of freedom for the *cis*/*trans* photoisomerization. TGA measurements on $\mathbf{3_{solv}}$ show a weight loss (ca. 4%) at ca. 50-60 °C and a corresponding endothermic event in the DSC at 62°C, indicating the presence of crystallization solvent; the solid is stable up to melting (T_{DSC} = 131 °C), which means that molecules of **3** are arranged in a robust framework. The solvent molecules must be distributed in the large cavities within the structure, but the amount of solvent is probably non-stoichiometric and with a high percentage of empty pores that could vary from crystal to crystal; collecting data at low temperature did not help in the detection of solvent in the structure. Molecules of **3** are found in their enol form in all the forms characterized here (**3A**, **3B** and $\mathbf{3_{solv}}$), as deduced from selected bond lengths (Table 1); no relevant variations of bond length and torsion angles are found by comparison between LT and RT crystallographic determinations.

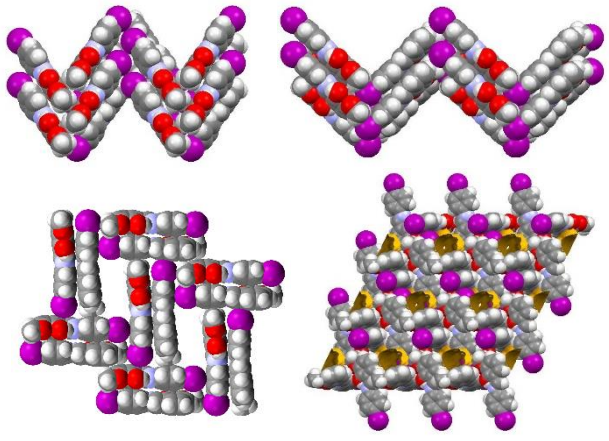

Figure 4. Herring-bone motifs and π-stacking in crystalline **3A** (top left; only the main image of disorder is shown), **3B** (top right, isomorphous with **2**) and $\mathbf{3_{solv}}$ (bottom left and bottom right); the yellow contour surfaces represent the large pores probably occupied by solvent in non-stoichiometric amount.

Solid solution of 2 and 3. Solids **2** and **3B** are isomorphous, *i.e.* they crystallize in the same space group with similar cell parameters, and differ only for the type of halogen atom; isomorphous compounds are usually able to form solid solution, in various ranges of composition. In order to explore the relative influence of bromine and iodine on the photochromic behaviour of **2** (see the photochromism section) we tried to prepare a 1:1 solid solution. Single crystals of the resulting product turned out to contain a larger amount of the bromine derivative, corresponding to the formula $\mathbf{2}_{0.7}\mathbf{3}_{0.3}$. The solid solution is isomorphous with the pure bromine and iodine parent compounds (see Table 1); the bromine and iodine atoms are disordered over the entire structure.

*Co-crystals of **1**, **2** and **3** with **I2F4***

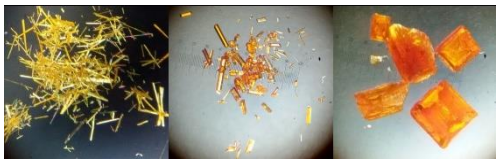

Figure 5. Single crystals of compounds $\mathbf{1}_2$**·2F4** (left), $\mathbf{2}_2$**·I2F4** (middle) and $\mathbf{3}_2$**·I2F4** (right), obtained by recrystallization from solution of the mechanosynthesis products (see Experimental).

Co-crystal 1_2·I2F4 . Yellow-orange needles have been obtained upon recrystallization of the as synthesized ground powder product from EtOAc/cyclohexane. They belong to the monoclinic crystal system, $P2_1/n$ space group (Table S3)**,** with one molecule of **1** and half a molecule of **I2F4** in the asymmetric unit. The only observed tautomeric form, both at room and low temperature, is the enol one, as deduced from bond lengths (Table 1). Molecules are twisted with Φ = 34.3° (**T1** = 32.8(6)°). By comparing torsion angles **T1** and **T2** in crystalline **1** and in the co-crystal **1_2·I2F4,** no relevant change in the overall shape of compound **1** molecules is detected. In the crystal structure one molecule of **I2F4** binds two molecules of **1** via halogen bonds of the I···$N_{(pyridine)}$ type. Piles of molecules of **1** are stacked in a *segregated* fashion along the *a*-axis (see Figure 5, left).

Co-crystal 2_2·I2F4 . Orange prisms have been obtained after recrystallization of the as-synthesized ground powder product from EtOAc/cyclohexane. They belong to the monoclinic crystal system, with $P2_1/n$ as space group. The observed tautomeric form (both at room and low temperature) is the enol form, as deduced from bond distances. As seen for the previously presented structures, the **T2** torsion angle is near-planar and the **T1** torsion angle exhibits a value of about 36.1(7)° at RT and of 35.4(5)° at LT. Measured value of Φ is of about 34.4° (RT) and 33.0° (LT). The crystal structure is characterized by a layered network in which molecules within the same layer interact edge-to-face, and interlayer forces are mainly due to edge-to-face stacking between molecules of **2** and to a *mixed-stacking* involving **I2F4** and the salicylidene moiety of **2** (Figure 5, middle). Directional interactions of the I···$O_{(hydroxyl)}$ type are also present (structure parameters are provided in Table S4).

Co-crystal 3_2·I2F4 . Orange prisms suitable for X-ray diffraction have been obtained after recrystallization of the as synthesized powder product from EtOAc/cyclohexane. They are isostructural with **2_2·I2F4** (Figure 5, right)**.** The observed tautomeric form (both at room and low temperature) is the enol form, as deduced from bond distances (see Table 1).

Solid-state NMR

The tautomerism and the halogen bond (XB) occurrence were investigated by ^{13}C and ^{15}N CPMAS solid-state NMR experiments. The SSNMR technique is known for providing clear evidence of the tautomeric state of a molecule thanks to its multinuclear approach based on the analysis of the ^{1}H, ^{13}C and ^{15}N nuclei. Indeed, their chemical shift strongly depends on the position of both double bonds and protons. Several examples of solid-state NMR and diffraction investigations of tautomeric and desmotrophic systems such as pyrazoles and pyrazolinones[35–38] are reported in the literature.[39] Recently, the tautomeric state of Pigment Yellow 138 has been investigated by solid-state 1D and 2D multinuclear NMR experiments and direct evidence of the presence of the NH-tautomer was provided by ^{1}H-^{14}N HMQC solid-state NMR at very fast MAS. 2-thiobarbituric acid is a

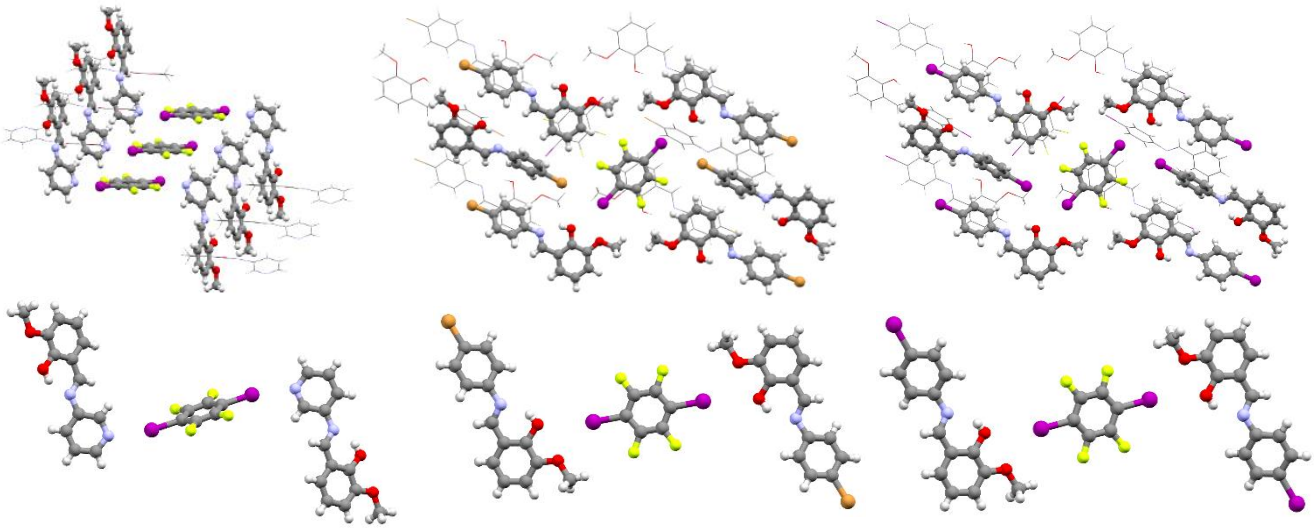

Figure 6. Molecular relative arrangements in crystalline 1_2·I2F4 (left), 2_2·I2F4 (middle) and 3_2·I2F4 (right, isomorphous with 2_2·I2F4) and relevant interactions involving halogen atoms in the three co-crystals (bottom).

representative case because both polymorphism and tautomeric polymorphism have been found and studied by X-ray crystallography as well as by ^{1}H, ^{13}C and ^{15}N CPMAS NMR.[40] This method was also successfully applied to determine the tautomeric state of the poorly crystalline phases III (HT-form)[41] and IV[42] of barbituric acid. In a similar approach also the XB occurrence can be easily probed by SSNMR by looking at the shifts of the nuclei involved in the interaction such as halogen atoms, ^{13}C and ^{15}N.[28,43,44]

The ^{13}C (with relevant assignments) and ^{15}N CPMAS spectra are reported in Figure 6 and Figure 7, respectively. The ^{15}N chemical shifts with assignments are listed in Table 2.

Concerning the starting compounds (**1**, **2** and **3$_{solv}$**) and the co-crystals (**1$_2$·I2F4**, **2$_2$·I2F4** and **3$_2$·I2F4**), the ^{13}C chemical shifts of the C-OH and of the N=CH atoms as well as the ^{15}N chemical shift of the N=C atom are consistent with the enol form. At room temperature, all structures are characterized by the N···H-O interaction as confirmed by the ^{15}N chemical shift of the N=CH atom around 285 ppm. The shifts observed upon co-crystal formation can be mainly related to packing effects rather than N···O distances variations (see X-ray data). In the ^{13}C CPMAS spectra, the number of signals is consistent with one independent molecule (Z'=1) for all samples but for **3,** which is characterized by two sets (or much broader peaks) of resonances in agreement with two independent molecules in the unit cell (Z'=2) as found by X-ray diffraction.

In **1$_2$·2F4**, the occurrence of a XB involving the pyridine nitrogen (N_{py}) atom has been easily verified by the ^{15}N CPMAS spectrum (Figure 7). Indeed, the N_{py} signal undergoes a low frequency shift, from 318.4 to 304.6 ppm upon co-crystallization of **1** with **I2F4** clearing indicating the XB formation (Figure 7). Similar shifts have been already reported not only for HB and XB formation but also upon metal coordination in agreement with the minor contribution of the lone pair to σ^{p}_{loc} since removed by quaternization.[44–48]

Table 2. Room temperature ^{15}N chemical shifts with assignments for compounds **1**, **2** and **3$_{solv}$** and their co-crystals **1$_2$·I2F4**, **2$_2$·I2F4** and **3$_2$·I2F4**

Sample	δ ^{15}N	Note
1	318.4	N_{py}
	282.4	C=N···H-O
1$_2$·I2F4	304.6	N_{py}···I
	279.2	C=N···H-O
2	277.0	C=N···H-O
2$_2$·I2F4	290.3	C=N···H-O
3$_{solv}$ [a]	286.9	C=N···H-O
3$_2$·I2F4	288.9	C=N···H-O

[a] two molecules in the asymmetric unit.

The formation of the XB interaction is also confirmed in the ^{13}C CPMAS spectrum by the high-frequency shift of the C-I resonance from 77.0 ppm (pure **I2F4**) to 79.3 ppm (**1$_2$·I2F4**). This is in agreement with the lengthening of the C-I bond (from 2.075 to 2.095 Å) and it is consistent with previously reported shifts. Interestingly, the shift of the C-I peak observed for **2$_2$·I2F4** and **3$_2$·I2F4** is in the opposite direction, toward lower frequencies (from 77.0 ppm for pure **I2F4** to 74.4 and 74.5 ppm, respectively).

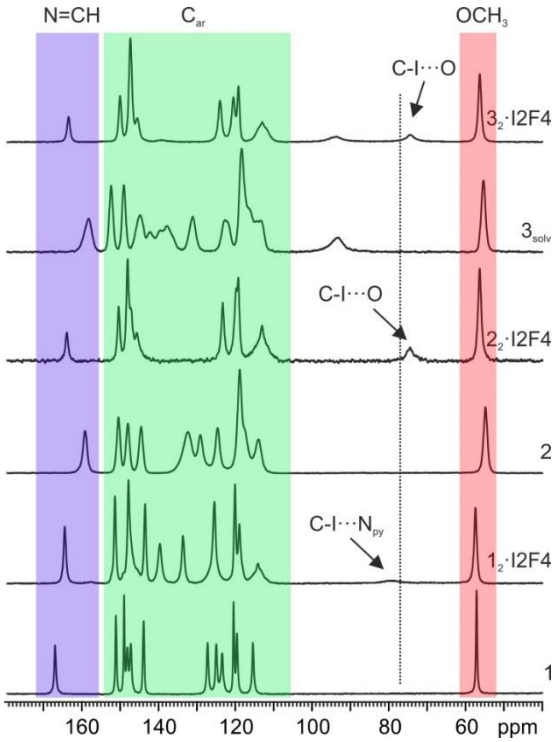

Figure 7. Room temperature ^{13}C (150.91 MHz) CPMAS spectra with relevant assignments of compounds **1**, **2** and **3$_{solv}$** and their co-crystals **1$_2$·I2F4**, **2$_2$·I2F4** and **3$_2$·I2F4**, recorded at 20 kHz. The dotted line represents the position of the C-I signal of pure **I2F4**.

This is an indication that the XB interaction is very weak as confirmed also by the long I···O distances (I···O_{CH3}= 3.264 and 3.243 Å for **2$_2$·I2F4** and **3$_2$·I2F4**, respectively compared to **1$_2$·I2F4**, I···N_{py}= 2.878 Å) and the poor directionality (C-I···O_{CH3}= 140.7 and 145.1° for **2$_2$·I2F4** and **3$_2$·I2F4**, respectively compare to **1$_2$·I2F4**, C-I···N_{py}=168.9°). Thus, the ^{13}C chemical shift is more influenced by packing effects than by the polarization induced by the XB. In other words, it seems that the driving force for the co-crystal formation for **2$_2$·I2F4** and **3$_2$·I2F4** is the packing efficiency rather than the XB interaction formation.

Thermochromic and photochromic behavior

The crystals of N-salycilideneanilines have been historically divided into two groups: thermo- and photochromic ones. Thermochromic crystals were defined as deeply colored at room temperature and pale yellow as the temperature is lowered. Whereas, photochromic crystals are pale yellow and they turn red, when irradiated with UV light.[49] Generally, a compact crystal packing determines purely thermochromic solids whereas photochromism is observed for open crystal packings. However, recent works on N-salicylideneanilines and on N–salicylideneaminopyridines (as single component systems, and as co-crystals or salts) revealed that a dense crystal packing

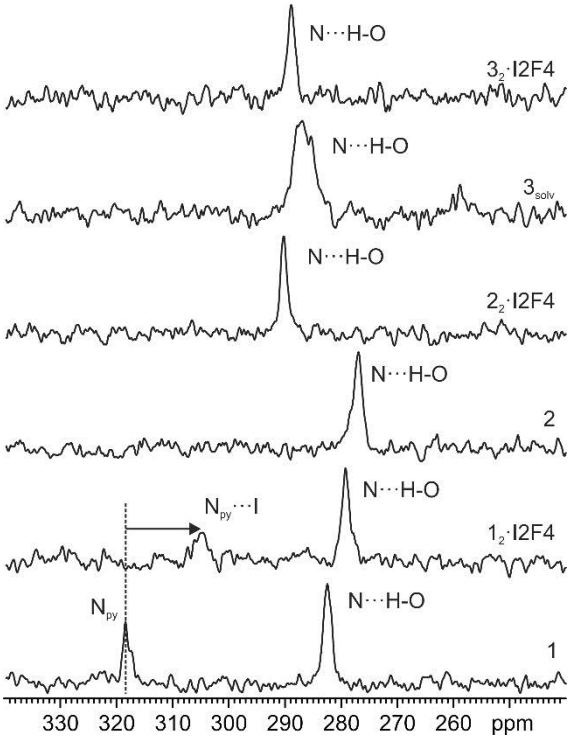

Figure 8. Room temperature ^{15}N (60.81 MHz) CPMAS spectra of compounds **1**, **2** and **3solv** and their co-crystals **1₂·I2F4**, **2₂·I2F4** and **3₂·I2F4**, recorded at 12 kHz.

could, sometimes, lead to photochromism as well.[9,10] Moreover, it is also true that photochromism and thermochromism are not mutually exclusive as thought before.[9,11,20] Besides this, Harada *et al*. reported that the temperature induced shift of the tautomeric equilibrium (thermochromism) could not be the unique cause of the color change as it also depends on an increase of fluorescence intensity, dominating the resulting visual color at low temperature in some cases.[49]

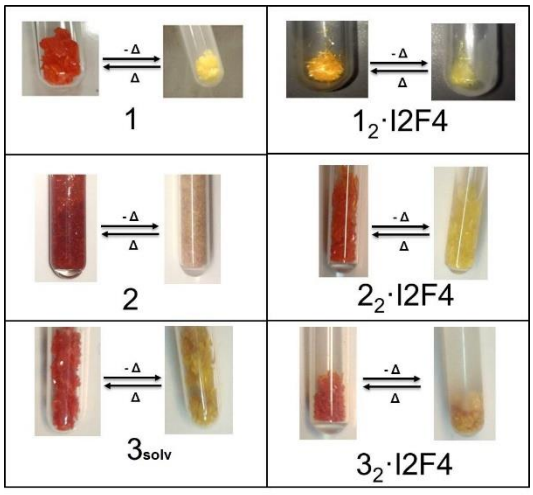

Figure 9. The qualitative, visual comparison of colour change for crystals and co-crystals of **1**, **2** and **3solv**, before (left) and after (right) immersion in liquid nitrogen.

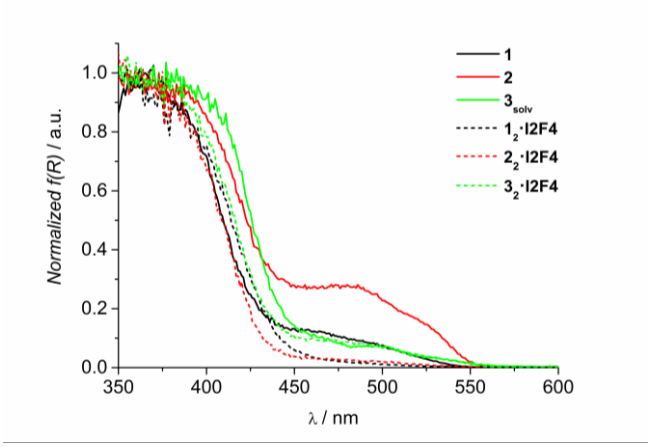

Figure 10. Normalized absorption spectra of powder samples of compounds **1**, **2**, **3solv** and respective co-crystals.

Absorption and emission properties of solid compounds **1**, **2**, **3solv** and co-crystals **1₂·I2F4**, **2₂·I2F4** and **3₂·I2F4**, both as crystals and as powders (ground crystals), have been determined at room temperature and upon cooling at 77K, in order to assess their thermochromic behavior, which could be qualitatively observed comparing vials of all crystalline materials before and after plunging them in liquid nitrogen (see Figure 8).

Photochromism was instead investigated by absorption and emission spectroscopy or by FTIR spectroscopy upon irradiation at 365 nm. For solids which shown photochromism, both kinetics of the photochemical back reaction (upon excitaton of the samples at 546 nm) and thermal fading (by leaving the samples in the dark at room temperature) were investigated.

Absorption spectra of powder samples of compounds **1**, **2**, **3solv** and relevant co-crystals are shown in Figure 9 (the same comparison is reported in Figure S4 for crystal samples). The spectra of **1**, **2**, and **3solv** show two distinct broad absorption bands, one extending below 430 nm and the other in the 430-550 nm region. The two bands can be ascribed to π-π* absorption of the enol form and of the thermally populated *cis*-keto form of the compounds, respectively, in analogy with literature reports.[8,10,49–51] The presence of the band around 470 nm testifies the existence of the *cis*-keto tautomer at room temperature even if this was not identified by other characterization techniques (X-ray diffraction and NMR measurements in the solid state).[5] A similar discrepancy has been reported in some cases[52,53] and can be attributed to a high absorption coefficient of the *cis*-keto form.[54] The spectra of the co-crystals show similar features, with a reduction of the contribution of the band at 470 nm in particular for **1₂·I2F4** and **2₂·I2F4**. The absorption spectra of the samples in their crystal form (Figure S4) show a different intensity distribution of the bands, with an apparent amplification of the absorption in the 430-550 nm range. The latter can derive from a flattening of the spectrum in the region of high absorption ($\lambda < 430$ nm) and intensification in the long wavelength range where the absorption is weaker due to optical effects, related to scattering and reflection, occurring in the large size (mm regime) crystals.[55]

Room temperature emission spectra of compounds **1**, **2**, **3$_{solv}$** and respective co-crystals are reported in Figure 10 for powder samples and in Figure S5 for crystal samples. Identical emission spectral features were obtained upon excitation both in the 350-430 nm and in the 430-550 nm regions. Excitation spectra collected at 650/660 nm (reported in Figure S6 and S7 for powders and crystals, respectively) overlap both absorption bands with similar relative intensity. The observed emission can therefore be ascribed to fluorescence of the *cis*-keto tautomer, obtained either *via* direct excitation of the thermally equilibrated *cis*-keto form or by excitation of the enol tautomer, followed by an excited state intramolecular proton transfer (ESIPT) process.[4] We had no evidence of enol emission below 500 nm, as generally observed for salicilideneaniline derivatives, due to the fast kinetics of the ESIPT process, occurring in the sub-ps/few ps time regime in the solid state.[56,57]

A comparison of the emission features of compounds **1**, **2**, **3$_{solv}$** and their co-crystals reveal similar spectra within the two series. Simple compounds **1**, **2** and **3$_{solv}$** show maxima at ca. 600 nm while co-crystals fluorescence is red-shifted by 10-20 nm (Figure 10 and S5 and Table 3), indicating a general excited state stabilization effect due to co-crystallization. Absolute emission quantum yields were found to be below the limit of detection of our system (2%) and single exponential decays with lifetimes of few hundreds of ps were measured for all compounds (Table 3). The latter data confirm the nature of the emission as resulting from the low-lying singlet excited state of the *cis*-keto tautomer.[56,57] A general trend in lifetime decrease is observed when moving from simple compounds to co-crystals (Table 3), likely due to an external heavy atom effect induced by the halogenated coformer.[26]

Emission properties of compounds **1**, **2**, **3$_{solv}$** and respective co-crystals were further investigated at 77 K in both powder and crystal samples. The emission spectra (Figure 11 and S8 for powders and crystals, respectively) show features similar to those observed at room temperature, with a higher spectral resolution. In particular, in the 540-590 nm region, a clear band appears in place of the weak shoulder detected at room temperature and blue-shifted by ca. 10 nm with respect to it (Table 3). The appearance of a blue shifted emission peak at low temperature, observed in similar systems, has been interpreted in terms of an emissive *cis*-keto excited state characterized by a distorted and less stable conformation. This conformation is quenched at room temperature due to a fast relaxation to the more stable planar

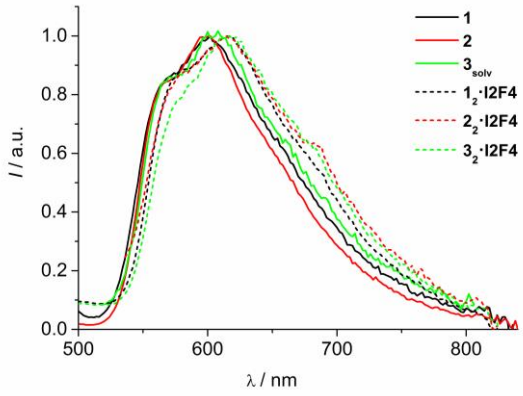

Figure 11. Normalized room temperature emission spectra of powder samples of compounds **1**, **2**, **3$_{solv}$** and respective co-crystals. λ_{exc} = 480 nm.

excited state responsible for emission in the longer wavelength region.[4,49,58] The bi-exponential behaviour of the emission decay observed on the whole spectral region for all the examined

Table 3. Fluorescence data at room temperature and 77 K for powder samples (in square brackets values for single crystal samples).

	298 K		77K	
	λ_{max} / nm[a]	τ / ps[b]	λ_{max} / nm[a]	τ / ps[b]
1	568 sh, 600 [574 sh, 602]	344 [344]	558, 598, 646 sh [558, 600, 642 sh]	185 (15%), 693 (85%) [273 (30%), 858 (70%)]
2	568 sh, 598 [572 sh, 598]	508 [511]	556, 594, 644 sh [558, 594, 642 sh]	164 (5%), 1328 (95%) [158 (5%), 1358 (95%)]
3$_{solv}$	570 sh, 606 [578 sh, 610]	175 [180]	558, 602, 650 sh [560, 604, 652 sh]	205 (30%), 674 (70%) [314 (55%), 896 (45%)]
1$_2$·I2F4	580 sh, 616 [584 sh, 616]	191 [210]	570, 610, 664 sh [570, 610, 662 sh]	204 (60%), 436 (40%) [262 (70%), 713 (30%)]
2$_2$·I2F4	580 sh, 614 [580 sh, 616]	133 [113]	574, 612, 662 sh [572, 608, 656 sh]	176 (50%), 401 (50%) [240 (50%), 456 (50%)]
3$_2$·I2F4	584 sh, 614 [580 sh, 618]	97 [98]	576, 616, 668 sh [578, 618, 670]	180 (30%), 334 (70%) [212 (70%), 454 (30%)]

[a] From corrected emission spectra. [b] Fluorescence lifetimes, excitation at 407 nm.

compounds (Table 3) corroborates the existence of a conformational change in the excited states of the *cis*-keto form in the present case. The emission spectra of the co-crystals are bathochromically shifted by 10-20 nm compared to those of the parent compounds, similarly to the room temperature behaviour. Low temperature excitation spectra collected at 600-620 nm show a pronounced depression of the 430-550 nm absorption region with respect to the same spectra collected at room temperature (see Figure S9 and S10 and, as one representative comparison, Figure S11). This behaviour, responsible of the yellowing of the colour of the samples at low temperature observable with the naked eye, is due to the decrease of the population of the *cis*-keto tautomer in the ground state. The low temperature, indeed, inhibits the thermal enol-keto tautomerism and suppresses the formation of the *cis*-keto form, absorbing in the 430-550 nm region. The observed emission, ascribed to the excited *cis*-keto tautomer, is a result of the fast ESIPT process that follows excitation of the enol tautomer, which is operative also at low temperature (a barrierless or proton tunnelling process has been suggested).[52,56] By comparison of room temperature and 77 K excitation spectra we can conclude that all the examined compounds and co-crystals exhibit thermochromism.

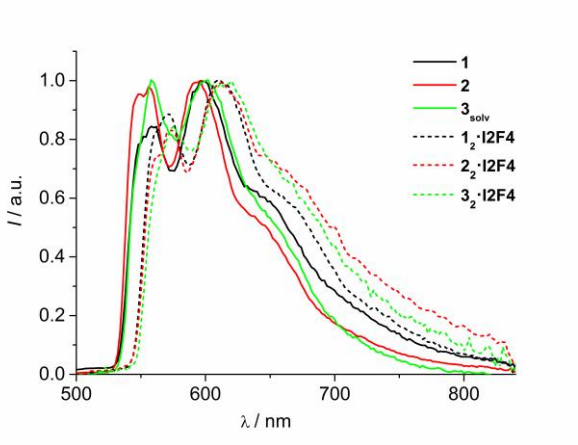

Figure 12. Normalized emission spectra at 77 K of powder samples of compounds **1**, **2**, **3$_{solv}$** and respective co-crystals. λ_{exc} = 450 nm.

The photochromic behavior of powder samples of compounds **1**, **2**, **3$_{solv}$** and of the corresponding co-crystals has been investigated by irradiating the samples at 365 nm (see the Experimental Section for details). While irradiation of compounds **1**, **1$_2$·I2F4** and **3$_{solv}$** did not produce appreciable changes in their absorption spectra (see Figure S13), the same experiment for **2**, **2$_2$·I2F4** and **3$_2$·I2F4** brought significant variations in the absorption spectral features. For these compounds the emission behavior upon excitation at 400 nm has been analyzed as a function of the irradiation time. Figure 12 shows the absorption and emission spectral changes observed for co-crystal **3$_2$·I2F4** upon irradiation at 365 nm (the results of analogous experiments for **2** and **2$_2$·I2F4** are reported in Figure S14 and S15). Irradiation causes an increase of absorption in the 450-600 nm region, reaching a photostationary state after 40 minutes of exposure (Figure 12a, S14a and S15a). The observed variation can be ascribed to the appearance of the absorption contribution of the *trans*-keto tautomer, formed as a result of an enol→*trans*-keto photoreaction, in the longer wavelength range of the spectrum (500-600 nm).[9,12,13,59]

The emission spectrum evolves with a change in the relative intensity of the bands, i.e. an increase in the 600-800 nm region at the expense of the shoulder at 560-570 nm (Figure 12b, S14b and S15b; the spectra have been arbitrarily scaled to better visualize changes in the intensity ratio). Excitation spectra collected at 575 nm and 650 nm in the photostationary state (Figure S16) evidence that absorption in the 450-600 nm contributes to a larger extent to emission at 650 nm. The emission emerging in the 600-800 nm region can therefore be safely ascribed to the *trans*-keto form of the investigated N-salicylidene anilines. Emission lifetimes measured for $\lambda > 650$ nm in the photostationary state (449 ps, 126 ps and 97 ps for **2**, **2$_2$·I2F4** and **3$_2$·I2F4**, respectively) were found to be very similar to those obtained before irradiation (see reference with values reported in Table 3). Among the three photochromic compounds, co-crystal **3$_2$·I2F4** is the one showing the largest spectral changes due to photoisomerization.

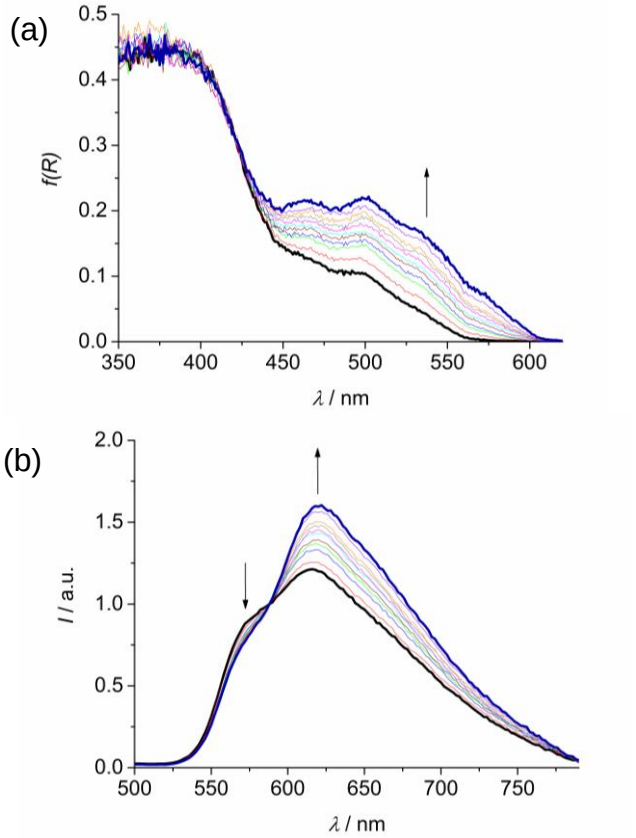

Figure 13. Absorption (a) and emission (b) spectra of **3$_2$·I2F4** before (black thick) and after (blue thick) irradiation at 365 nm for 40 min (20 min LP and 20 min HP, see Experimental Section for details). Thin lines represent spectra at intermediate times. In (b) the spectra are arbitrarily normalized at 588 nm; λ_{exc} = 400 nm.

As a mechanism of the photochromic reaction it has been suggested that, upon excitation of the enol form and proton transfer, the excited distorted keto intermediate can deactivate either to the lower lying *cis*-keto and to the *trans*-keto excited states, being precursor of both.[52,58] Emission from the

photogenerated *trans*-keto tautomer has been anyway rarely reported.[10,53,60,61]

The initial absorption spectra of **2**, **2_2·I2F4** and **3_2·I2F4** are completely recovered either photochemically, upon excitaton of the samples at 546 nm or thermally, by leaving the samples in the dark at room temperature. Figure S17-S19 show spectral and kinetic features of the recovery processes. While photochemical back reactions are characterized by a bi-exponential behaviour, the thermal fading processes are well described by first order reactions. A two-stage thermal decay of the *trans*-keto form of anils in the solid state has been previously reported.[9,12,13,62] It can be noticed that the two co-crystals show much faster back reactions compared to simple compound **2**: the photoconversion kinetics of the *trans*-keto tautomer are of the order of tens of seconds for **2_2·I2F4** and **3_2·I2F4** and tens of minutes for **2** (Figure S17-S19). Concerning the thermal fading, conversion times of 604 min, 65 min and 186 min have been measured for the *trans*-keto form of **2**, **2_2·I2F4** and **3_2·I2F4** respectively, confirming that **2** undergoes the slowest process.

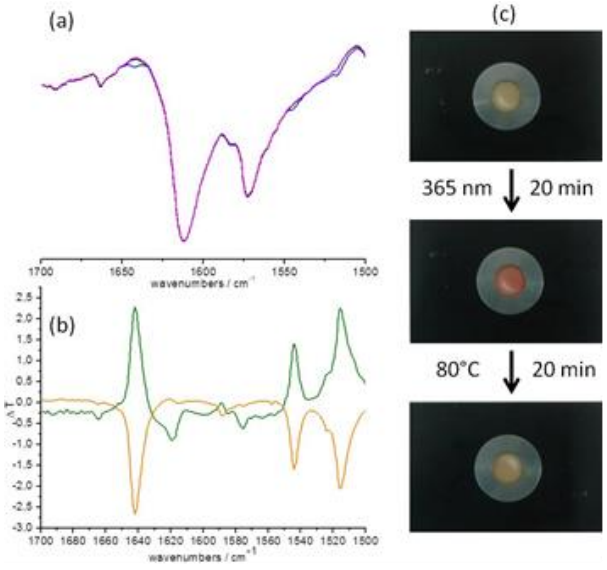

Figure 14. FTIR spectroscopy for 2_2·I2F4 dispersed in KBr pellets: (a) IR spectra of the untreated sample (black), after 20 min irradiation at 365 nm (blue) and after thermal recovery (magenta). (b) Difference spectra between the untreated and the irradiated sample (green) and between the irradiated and the thermal recovered one (orange). (c) Pictures taken on the KBr pellets used for the FTIR measurements.

FTIR spectroscopy measurements are in agreement with the photochromic behaviour observed in absorption and emission spectroscopy, but they also add new information concerning the polymorphic modifications of compound **3_{solv}** (**3A** and **3B**) and the **$2_{0.7}3_{0.3}$** solid solution. Of all crystalline materials under study only compound **2** and the co-crystals **2_2·I2F4** and **3_2·I2F4** clearly display a photochromic behaviour. It is worth noting that **2** represents a positive violation of the dihedral angle Φ rule, while crystalline **1** and its co-crystal **1_2·I2F4** represent a negative one since they are non photochromic despite suitable values of Φ. The photochromic behaviour of compound **3**, in its polymorphic modifications **3A** and **3B**, was also investigated *via* FTIR spectroscopy: both **3A** and **3B** were found to be non-photochromic, although **3B**, being isomorphous with **2**, was expected to behave similarly. The **$2_{0.7}3_{0.3}$** solid solution was also examined by FTIR, and the effect of the presence of iodine in the same crystal with bromine evaluated: the solid solution turned out to be *non* photochromic, *i.e.* the presence of a lower amount of iodine with respect to bromine seems sufficient to switch off the photochromic behaviour.

For those compounds which showed photochromism the general behavior is as follows: FTIR spectra collected before and after 20 min irradiation at 365 nm present some variations which are in agreement with the formation of the *trans-keto* form.[11,63] The band around 1612 cm^{-1} (ascribed to the C=N stretching of the *enol* form) decreases, and the small band around 1642 cm^{-1} (due to the C=O stretching of the *trans-keto* tautomer) appears. After thermal treatment (80°C, 20 min) the original spectrum is recovered, indicating the reversibility of the process. The two processes are mirrored in the color change from yellow to orange upon irradiation, and to yellow again after thermal treatment (80°C, 20 min). This behaviour is shown in Figure 13 for the co-crystal **2_2·I2F4**; Figure S23-S24 in the ESI file show the behaviour of all the other compounds discussed in the present work.

Conclusions

In conclusion, we have used a co-crystal strategy to modulate thermochromism and photochromism in a series of selected N-salicylideneanilines and N-salicylideneaminopyridines.

Mechanosynthesis allowed formation of the desired products with high yield and no need to use further solvent-based methods. In the case of compound **3**, the solid **3A** is selectively obtained. Recrystallization of powder of **3A** (as synthesized product) yielded two new crystal forms: **3B** (toluene, isostructural to **2**) and **3_{solv}** (EtOAc solvate). Such a tendency toward the formation of multiple crystal forms has not been observed for **2**.

Halogen bonding interactions of various strength are found within the presented crystal structures: particular attention has been given to the role of the C-I···$O_{(hydroxyl)}$ interaction in affecting the enol/*cis*-keto tautomerism. Contrary to what has been proven for the intermolecular C-OH···$O_{(hydroxyl)}$ hydrogen bond, the C-I···$O_{(hydroxyl)}$ halogen bond does not displace the ground state enol/*cis*-keto balance toward the *cis*-keto form, neither at room nor at low temperature. This can be seen as a clear advantage in the construction of thermochromic solids given that supramolecular effect of formation of an intermolecular H-bond could reduce the color variation of anil-based systems.[64]

All crystal forms present a strong thermochromic behavior (from yellow-orange to pale yellow by lowering the temperature) and, in addition, some of them (crystalline **2, 2_2·I2F4** and **3_2·I2F4**) are also photochromic, although several studies in the field report that these properties are mutually exclusive. In all systems, photochemical back reaction and thermal fading process are well described as a bi-exponential and as a first order reaction, respectively.

Both negative (crystalline **1**, **1_2·I2F4**) and positive (crystalline **2**) violations of the dihedral angle-based rule have been found. It is also noteworthy that crystals, **2** and **3B,** despite their isostructurality**,** do not show the same chromic behavior although they were expected to behave similarly. In fact, **2** is photochromic whereas **3B** does not show such a behaviour**.** What is even more remarkable is that the combination of compound **2** and **3** in a **$2_{0.7}3_{0.3}$** solid solution (isostructural to solids **2** and **3B**) leads to a

non-photochromic solid. We speculate that this effect can in part be due to the hindering effect of the large iodine atom on the free pedal motion in the tight $P2_12_12_1$ packing. A similar trend is observed for **2_2·I2F4** and **3_2·I2F4** co-crystals**.** In this case the *p*-iodine substituent is not big enough to turn photochromism off but it is enough to slow down, of about three times, the thermal fading process. For **2_2·I2F4** and **3_2·I2F4** co-crystals, the ability to undergo photoisomerization is increased with respect to **2** as confirmed by the fact that their photochemical back reaction (tens of seconds for **2** and tens of minutes for **2_2·I2F4** and **3_2·I2F4** respectively) and thermal fading process (of about 604 min, 65 min and 186 min for **2**, **2_2·I2F4** and **3_2·I2F4** respectively) are much faster. This is consistent with a structure opening effect made by the insertion of the co-crystal former (**I2F4**) in the structure.
These results reveal how subtle structure changes can dramatically affect the solid-state photochromic behaviour and highlight how empirical rules, based only on structural considerations, are not suitable for the rationalization/prediction of photochromism.

Experimental Section

Materials. *ortho*-Vanillin (*2-Hydroxy-3-methoxybenzaldehyde*), 3-aminopyridine, 4-bromoaniline and 4-iodoaniline were sourced from Sigma-Aldrich (Steinheim, germany) (>99% chemical purity) and used as received. Solvents used for crystallization (EtOH, EtOAc, cyclohexane and toluene from Acros Organic, Geel, Belgium) are commercially available and were used without further purification.

Synthesis of the compounds
All N-salicylideneanilines, N-salicylideneaminorpiridines and their co-crystals were synthesized by mechanosynthesis.[9,65,66] Dry grinding was performed with a Retsch MM 400 Mixer Mill, equipped with two grinding jars in which five 2 mL Eppendorf tubes can be installed with 8−10 stainless steel grinding balls (1 mm diameter) in a sample.

Synthesis of 1. (E)-2-methoxy-6-(pyridin-3-yliminomethyl)phenol. The title compound was synthetized by dry grinding of equimolar amounts of 3-aminopyridine and *ortho*-vanillin. Powder X-ray diffraction (PXRD) analysis highlights the presence of new peaks due to the formation of the Schiff base product. Residual peaks of both reactants are not observed in the ground product confirming a near-total conversion (Figure S25a). Orange prisms of compound **1**, suitable for X-ray analysis, have been obtained by slow evaporation from a saturated solution in ethyl acetate after 4 days.
Synthesis of 2. 2-[(1E)-[(4-bromophenyl)imino]methyl]-6-methoxyphenol. The title compound was synthetized by dry grinding of equimolar amounts of 4-bromoaniline and *ortho*-vanillin. Powder X-ray diffraction (PXRD) analysis also highlights the presence of new peaks due to the Schiff base product formation. Residual peaks of both reactants are not observed in the ground product confirming a near-total conversion. Orange needles of compound **2**, suitable for X-ray analysis, have been obtained by slow evaporation from a saturated solution in ethyl acetate after 3 days.
Synthesis of 3A, 3B, 3_{solv}. 2-[(1E)-[(4-iodophenyl)imino]methyl]-6-methoxyphenol. The title compound was synthetized by dry grinding of equimolar amounts of 4-iodoaniline and *ortho*-vanillin. Powder X-ray diffraction (PXRD) highlights new peaks coming from the crystalline Schiff base product formed during grinding. Residual peaks of both reactants are not observed in the ground product confirming a near-total conversion. Recrystallization in several solvents was performed in order to obtain single crystals suitable for X-ray diffraction. Moreover, two polymorphs and a solvate form of **3** were obtained, depending on the crystallization conditions. Orange-red blocks of form **3A** were obtained by slow evaporation of a saturated solution in EtOH. Orange-red crystals of form **3B** were obtained by seeding with **2** a saturated solution in toluene, and leaving it to slowly evaporate, while orange-red prisms of form **3_{solv}** were obtained by recrystallization from ethyl acetate.
Comparison of the PXRD diffractogram of the ground powder, taken directly after synthesis, with PXRD diffractograms calculated on the basis of single crystal data for **3A, 3B** and **3_{solv},** reveals selective formation of form **3A** (Figure S25a).

Synthesis of the $2_{0.7}$-$3_{0.3}$ solid solution. Equimolar quantities of **2** and **3_{solv}** were dissolved in ethyl acetate; after 2 days crystals of suitable dimensions for X-ray diffraction were obtained by slow evaporation of solvent at room temperature.
Synthesis of 1_2·I2F4. Co-crystallization was achieved by grinding (120' at 30 Hz) of compound **1** and **I2F4** at a 2:1 molar ratio. Comparison of the PXRD diffractogram of the ground powder, taken directly after synthesis, with PXRD diffractogram calculated from the single crystal structure of **1_2·I2F4**, reveals selective formation of **1_2·I2F4** co-crystal (Figure S25b). Single-crystals suitable for X-ray diffraction were obtained by slow evaporation of saturated solutions in ethanol/cyclohexane. Orange-yellow needles have been obtained after 5 days.
Synthesis of 2_2·I2F4. Co-crystallization was performed by dry grinding (120' at 30 Hz) of compound **2** and **I2F4** in a 2:1 molar ratio. Comparison of the PXRD diffractogram of the ground powder, with PXRD diffractogram calculated from the single crystal structure of **2_2·I2F4**, highlights selective formation of 2:1 **2_2·I2F4** co-crystal. After recrystallization in ethanol/cyclohexane, orange prisms have been obtained.
Synthesis of 3_2·I2F4. Co-crystallization was performed by dry grinding (120' at 30 Hz) of compound **3** and **I2F4** in a 2:1 molar ratio. Comparison of the PXRD diffractogram of the ground powder, with the calculated PXRD diffractogram of **3_2·I2F4**, shows selective formation of 2:1 **3_2·I2F4** co-crystal. After recrystallization in ethanol/cyclohexane, orange prisms have been obtained after 4 days.

Characterization
FTIR spectroscopy. FTIR spectra were collected using a Bruker Alpha FTIR spectrometer. FTIR spectra in the range 1700-1500 cm^{-1} were run on KBr pellets (sample amount: 1-2 mg, KBr amount: 200 mg), resolution was set to 2 cm^{-1}, and 128 cycles for both background and measurement were collected. Spectra were run twice, before and after 20 min of UV irradiation (365 nm) on the same pellet sample, when a change in the color or in the spectrum was noticed, a further spectrum was measured after thermal treatment (pellet kept in the oven at 80°C for 20 minutes). Pellets were irradiated directly in the sample holder using 2 UV-LED (LED ENGINE LZ1-10UV00-0000, λ = 365 nm) placed at a distance of 1 cm each.
Crushed pellets were subjected to powder X-Ray diffraction analysis to exclude any solid state reaction triggered by pressure during pellet formation. As evidenced by powder patterns all crystalline materials resulted stable and did not react with KBr during pellet preparation (see ESI).
Solid-state NMR. Solid-state NMR experiments were acquired on a Jeol ECZR 600 instrument operating at 600.17, 150.91 and 60.81 MHz for ^{1}H, ^{13}C and ^{15}N nuclei, respectively. The samples were packed in a 3.2 mm rotor (volume = 50 μL) and spun at 20 and 12 kHz for ^{13}C and ^{15}N nuclei, respectively. All data were collected at ambient probe temperatures. All ^{13}C and ^{15}N experiments employed the RAMP-CP pulse sequence (^{1}H 90° pulse=2.189 μs, contact time = 9 and 4 ms, respectively) with the TPPM ^{1}H decoupling with an rf field of 75 kHz during the acquisition period. Detailed acquisition parameters may be found in the Supporting Information (Table S5). ^{13}C and ^{15}N chemical shift scales were referenced with the resonance of hexamethylbenzene (^{13}C methyl signal at 17.4 ppm), and glycine (^{15}N signal at 33.4 ppm with respect to NH_3), respectively as external standards.
Absorption and emission spectroscopy, photochemistry. Measurements were performed both on crystals as such and on gently crushed powder samples placed inside two quartz slides. Reflectance spectra of solid samples were acquired with a PerkinElmer Lambda 9

UV/Vis/NIR spectrophotometer equipped with a 60 mm integrating sphere and converted in absorption spectra using the Kubelka–Munk function.[67] Emission spectra were collected in front-face mode with an Edinburgh FLS920 fluorimeter equipped with a Peltiercooled Hamamatsu R928 PMT (200–850 nm), and corrected for the wavelength dependent phototube response. Absolute emission quantum yields were determined according to the method reported by Ishida et al.,[68] by using the same fluorimeter equipped with a 4 inch Labsphere integrating sphere. The limit of detection of the system is 0.020. Measurements at 77K made use of quartz capillary tubes immersed in liquid nitrogen contained in a home-made quartz Dewar. Band maxima and luminescence intensities are obtained with uncertainties of 2 nm and 10%, respectively. Fluorescence lifetimes were determined with an IBH 5000F time-correlated single-photon counting apparatus equipped with a TBX Picosecond Photon Detection Module by using a pulsed 407 nm laser diode (59 ps pulse width) powered by a Hamamatsu C4725 light pulser as excitation source. Analysis of the fluorescence decay profiles against time was accomplished with the Decay Analysis Software DAS6 provided by the manufacturer. The estimated error on lifetime determinations is 10%.

Photochromic investigations have been performed by irradiating a thin layer of the powder sample, placed inside two quartz slides, by using a collimated 100 W Hg arc lamp and selecting the desired spectral lines (365 or 546 nm) by means of bandpass interference filters. Forward reactions (λ_{irr} = 365 nm) made use of two different light powers: 2 mW cm^{-2} (low power: LP) and 20 mW cm^{-2} (high power: HP), the former obtained by using a neutral density filter. For back reactions (λ_{irr} = 546 nm) the light intensity was 5 mW cm^{-1}. Thermal fading was analyzed by a reflectance (%) time scan at a single wavelength (500 nm) performed with the spectrophotometer described above; the experimental conditions allowed for a close to dark environment.

Crystal Structure determination. Single-crystal diffraction data for **1**, **2**, $\mathbf{3_{solv}}$, $\mathbf{1_2{\cdot}I2F4}$, $\mathbf{2_2{\cdot}I2F4}$ and $\mathbf{3_2{\cdot}I2F4}$ were collected at RT and LT on a Gemini Ultra R system (4-circle kappa platform, Ruby CCD detector) using Mo Kα (λ = 0.71073Å) radiations. Single-crystal diffraction data for **3A**, **3B** and $\mathbf{2_{0.7}\text{-}3_{0.3}}$ were collected at RT on an Oxford X'Calibur S CCD diffractometer equipped with a graphite monochromator (Mo Kα radiation, λ = 0.71073Å). Selected crystals were mounted on the tip of a quartz pin using cyanoacrylate (commercial glue). Structures were solved by direct methods using the WinGX suite of programs[69] with Sir-2014[70] and then refined using either SHELX-97 or SHELXL-2014[71]. Non-hydrogen atoms were anisotropically refined and the hydrogen atoms (not implicated in H-bonds) in the riding mode with isotropic temperature factors fixed at 1.2 times U(eq) of the parent atoms. Hydrogen atoms implicated in hydrogen bonds were localized by Fourier difference maps. The solvent of crystallization in the structure of $\mathbf{3_{solv}}$ could not be unambiguously determined, therefore, the contribution of the solvent to the calculated structure factors was taken into account by using the SQUEEZE procedure of PLATON.[72] Positional disorder (70:30) in crystalline **3A** was treated by first refining the occupancy parameter of iodine, then fixing the occupancy factor and freely refining the thermal parameter. The whole minor image of disorder was located experimentally, but only the iodine atom was refined anisotropically. Disorder in the bromine/iodine position was treated analogously in the solid solution $\mathbf{2_{0.7}3_{0.3}}$. The program Mercury[73] was used for molecular graphics. Structures have been submitted to the Cambridge Structure Database[74] (CSD refcodes: 1407547, 1407548, 1456341, 1483225-1483232, 1523380-1523382)

Powder Diffraction Measurements. X-ray powder diffractograms in the 2θ range 5-40° (step size 0.02°; time/step, 20s; 40mA x 40kV) were collected on a Panalytical X'Pert PRO automated diffractometer equipped with a X'Celerator detector and in Bragg-Brentano geometry using Cu Kα radiation. The program Mercury[73] has been used for simulation of X-ray powder patterns from single crystal data.

Thermogravimetric Analyses (TGA). TGA measurements were performed with a Perkin-Elmer TGA7 in the temperature range 40 – 350 °C under N2 gas flow at a heating rate of 5.00 °C min-1.

Differential Scanning Calorimetry (DSC). DSC measurements were performed with a Perkin-Elmer PyrisDiamond DSC. Samples (3 – 5 mg) were placed in aluminum open pans. Heating was carried out at 5.00 °C min-1 for all samples, in the temperature range 40 – 140 °C.

Acknowledgements

CNR (Project "PHEEL"), MIUR-CNR project "Nanomax" N-CHEM, CNR-ASRT (Egypt) Bilateral Cooperation Project "FLUO-NanoFAB are aknowledged. Part of this work has been carried out on XRD equipment from the 'plateforme de Caractérisation PC2-UNamur'. The University of Bologna is also acknowledged (F.G, S.d.A and F.S). M.R.C. and R.B. are indebted with Jeol Company for helpful technical assistance and cooperation. We thank Dr. Katia Rubini for her help with DSC and TGA measurements. Tom Leyssens (Université Catholique de Louvain) and Benoît Champagne (Université de Namur) are gratefully acknowledged. A.C. is grateful to Bernadette Norberg for technical support. A.C. benefits from a F.R.S-FNRS ("Aspirant") grant. This work was published thanks to funding of 'Actions de Recherche Concertées' (ARC) de la Direction générale de l'Enseignement non obligatoire et de la Recherche scientifique – Direction de la Recherche scientifique – Communauté française de Belgique. This work was supported in part by the EU COSTAction CM1402 "Crystallize".

Keywords: thermochromism • photochromism • co-crystals • solid-state reactions • solid-state NMR

[1] J. Zhang, Q. Zou, H. Tian, *Adv. Mater.* **2013**, *25*, 378–399.

[2] S. Kawata, Y. Kawata, *Chem. Rev.* **2000**, *100*, 1777–1788.

[3] J. Cusido, E. Deniz, F. M. Raymo, *European J. Org. Chem.* **2009**, *2009*, 2031–2045.

[4] E. Hadjoudis, I. M. Mavridis, *Chem. Soc. Rev.* **2004**, *33*, 579–588.

[5] K. Ogawa, Y. Kasahara, Y. Ohtani, J. Harada, *J. Am. Chem. Soc.* **1998**, *120*, 7107–7108.

[6] J. Harada, H. Uekusa, Y. Ohashi, *J. Am. Chem. Soc.* **1999**, *121*, 5809–5810.

[7] J. Harada, K. Ogawa, *Chem. Soc. Rev.* **2009**, *38*, 2244–2252.

[8] K. Johmoto, T. Ishida, A. Sekine, H. Uekusa, Y. Ohashi, *Acta Crystallogr. Sect. B Struct. Sci.* **2012**, *68*, 297–304.

[9] A. Carletta, X. Buol, T. Leyssens, B. Champagne, J. Wouters, *J. Phys. Chem. C* **2016**, *120*, 10001–10008.

[10] F. Robert, A. D. Naik, B. Tinant, R. Robiette, Y. Garcia, *Chem. - A Eur. J.* **2009**, *15*, 4327–4342.

[11] K. M. Hutchins, S. Dutta, B. P. Loren, L. R. MacGillivray, *Chem. Mater.* **2014**, *26*, 3042–3044.

[12] I. O. Staehle, B. Rodríguez-Molina, S. I. Khan, M. A. Garcia-Garibay, *Cryst. Growth Des.* **2014**, *14*, 3667–3673.

[13] M. Sliwa, S. Létard, I. Malfant, M. Nierlich, P. G. Lacroix, T. Asahi, H. Masuhara, P. Yu, K. Nakatani, *Chem. Mater.* **2005**, *17*, 4727–4735.

[14] G. R. Desiraju, *Angew. Chemie Int. Ed.* **2007**, *46*, 8342–8356.

[15] G. R. Desiraju, *Angew. Chemie Int. Ed. English* **1995**, *34*, 2311–2327.

[16] D. Braga, F. Grepioni, *Making Crystals by Design : Methods,*

Techniques and Applications, Wiley-VCH, **2007**.

[17] K. Biradha, R. Santra, *Chem. Soc. Rev.* **2013**, *42*, 950–67.

[18] D. Braga, L. Brammer, N. R. Champness, *CrystEngComm* **2005**, *7*, 1–19.

[19] C. B. Aakeröy, N. R. Champness, C. Janiak, *CrystEngComm* **2010**, *12*, 22–43.

[20] P.-L. Jacquemin, K. Robeyns, M. Devillers, Y. Garcia, *Chem. - A Eur. J.* **2015**, *21*, 6832–6845.

[21] M. Zbačnik, M. Vitković, V. Vulić, I. Nogalo, D. Cinčić, *Cryst. Growth Des.* **2016**, *16*, 6381–6389.

[22] G. Cavallo, P. Metrangolo, R. Milani, T. Pilati, A. Priimägi, G. Resnati, G. Terraneo, *Chem. Rev.* **2016**, *116*, 2478–2601.

[23] J. Xu, X. Liu, J. K.-P. Ng, T. Lin, C. He, *J. Mater. Chem.* **2006**, *16*, 3540–3545.

[24] L. Meazza, J. A. Foster, K. Fucke, P. Metrangolo, G. Resnati, J. W. Steed, *Nat. Chem.* **2012**, *5*, 42–47.

[25] F. Grepioni, S. d'Agostino, D. Braga, A. Bertocco, L. Catalano, B. Ventura, *J. Mater. Chem. C* **2015**, *3*, 9425–9434.

[26] S. d'Agostino, F. Grepioni, D. Braga, B. Ventura, *Cryst. Growth Des.* **2015**, *15*, 2039–2045.

[27] H. Wang, R. X. Hu, X. Pang, H. Y. Gao, W. J. Jin, *CrystEngComm* **2014**, *16*, 7942–7948.

[28] M. Baldrighi, G. Cavallo, M. R. Chierotti, R. Gobetto, P. Metrangolo, T. Pilati, G. Resnati, G. Terraneo, *Mol. Pharm.* **2013**, *10*, 1760–1772.

[29] Z.-L. Jing, R.-N. Li, N. Yang, *Acta Crystallogr. Sect. E Struct. Reports Online* **2007**, *63*, o3001–o3001.

[30] C.-S. Zheng, N. Yang, M. Li, Z.-L. Jing, *Acta Crystallogr. Sect. E Struct. Reports Online* **2005**, *61*, o3613–o3614.

[31] P. Metrangolo, G. Resnati, *Chem. - A Eur. J.* **2001**, *7*, 2511–2519.

[32] D. Braga, L. Maini, F. Grepioni, *Chem. Soc. Rev.* **2013**, *42*, 7638.

[33] S. L. James, C. J. Adams, C. Bolm, D. Braga, P. Collier, T. Friščić, F. Grepioni, K. D. M. Harris, G. Hyett, W. Jones, A. Krebs, J. Mack, L. Maini, A. G. Orpen, I. P. Parkin, W. C. Shearouse, J. W. Steed, D. C. Waddell, *Chem. Soc. Rev.* **2012**, *41*, 413–447.

[34] E. Hadjoudis, M. Vittorakis, I. Moustakali-Mavridis, *Tetrahedron* **1987**, *43*, 1345–1360.

[35] M. Angeles García, C. López, R. M. Claramunt, A. Kenz, M. Pierrot, J. Elguero, *Helv. Chim. Acta* **2002**, *85*, 2763–2776.

[36] W. Holzer, R. M. Claramunt, C. López, I. Alkorta, J. Elguero, *Solid State Nucl. Magn. Reson.* **2008**, *34*, 68–76.

[37] J. Elguero, F. H. Cano, C. Foces-Foces, A. L. Llamas-Saiz, H. Limbach, F. Aguilar-Parrilla, R. M. Claramunt, C. López, *J. Heterocycl. Chem.* **1994**, *31*, 695–700.

[38] C. Foces-Foces, A. L. Llamas-Saiz, R. M. Claramunt, C. López, J. Elguero, *J. Chem. Soc. Chem. Commun.* **1994**, *118*, 49–1145.

[39] J. Elguero, *Cryst. Growth Des.* **2011**, 4731–4738.

[40] M. R. Chierotti, L. Ferrero, N. Garino, R. Gobetto, L. Pellegrino, D. Braga, F. Grepioni, L. Maini, *Chem. - A Eur. J.* **2010**, *16*, 4347–4358.

[41] D. M. Többens, J. Glinneman, M. R. Chierotti, J. van de Streek, D. Sheptyakov, *CrystEngComm* **2012**, *14*, 199–236.

[42] M. U. Schmidt, J. Brüning, J. Glinnemann, M. W. Hützler, P. Mörschel, S. N. Ivashevskaya, J. van de Streek, D. Braga, L. Maini, M. R. Chierotti, R. Gobetto, *Angew. Chemie Int. Ed.* **2011**, *50*, 7924–7926.

[43] C. M. Widdifield, G. Cavallo, G. A. Facey, T. Pilati, J. Lin, P. Metrangolo, G. Resnati, D. L. Bryce, *Chem. - A Eur. J.* **2013**, *19*, 11949–11962.

[44] M. Baldrighi, D. Bartesaghi, G. Cavallo, M. R. Chierotti, R. Gobetto, P. Metrangolo, T. Pilati, G. Resnati, G. Terraneo, *CrystEngComm* **2014**, *16*, 875–5904.

[45] R. Pettinari, F. Marchetti, C. Pettinari, F. Condello, B. W. Skelton, A. H. White, M. R. Chierotti, R. Gobetto, *Dalt. Trans.* **2016**, *45*, 5404–5404.

[46] M. R. Chierotti, R. Gobetto, *Chem. Commun.* **2008**, 1621-1634.

[47] I. Yavari, J. D. Roberts, *Magn. Reson. Chem.* **1979**, *12*, 87–91.

[48] P. Cerreia Vioglio, M. R. Chierotti, R. Gobetto, *CrystEngComm* **2016**, *18*, 9173–9184.

[49] J. Harada, T. Fujiwara, K. Ogawa, *J. Am. Chem. Soc.* **2007**, *129*, 16216–16221.

[50] T. Fujiwara, J. Harada, K. Ogawa, *J. Phys. Chem. B* **2004**, *108*, 4035–4038.

[51] G. M. Mercier, K. Robeyns, T. Leyssens, *Cryst. Growth Des.* **2016**, *16*, 3198–3205.

[52] E. Hadjoudis, A. Rontoyianni, K. Ambroziak, T. Dziembowska, I. M. Mavridis, *J. Photochem. Photobiol. A Chem.* **2004**, *162*, 521–530.

[53] M. Avadanei, V. Cozan, S. Shova, J. A. Paixão, *Chem. Phys.* **2014**, *444*, 43–51.

[54] J. W. Ledbetter, *J. Phys. Chem.* **1966**, *70*, 2245–2249.

[55] a) G. Kortüm, W. Braun, G. Herzog, Angew. Chemie Int. Ed. 1963, 2, 333–341. b) G. Kortüm, "Reflectance spectroscopy - Principles, Methods Applications" Springer-Verlag, Berlin - Heidelber - New York, 1969.

[56] S. Taro, T. Kobayashi, T. Inabe, *J. Phys. Chem. A* **1997**, *101*, 644–649.

[57] M. Sliwa, N. Mouton, C. Ruckebusch, S. Aloïse, O. Poizat, G. Buntinx, R. Métivier, K. Nakatani, H. Masuhara, T. Asahi, *J. Phys. Chem. C* **2009**, *113*, 11959–11968.

[58] D. Higelin, H. Sixl, *Chem. Phys.* **1983**, *77*, 391–400.

[59] D. A. Safin, K. Robeyns, M. G. Babashkina, Y. Filinchuk, A. Rotaru, C. Jureschi, M. P. Mitoraj, J. Hooper, M. Brela, Y. Garcia, *CrystEngComm* **2016**, *12*, 106.

[60] D. A. Safin, M. G. Babashkina, K. Robeyns, Y. Garcia, *RSC Adv.* **2016**, *6*, 53669–53678.

[61] F. Robert, P.-L. Jacquemin, B. Tinant, Y. Garcia, *CrystEngComm* **2012**, *14*, 4396.

[62] K. Johmoto, A. Sekine, H. Uekusa, *Cryst. Growth Des.* **2012**, *12*, 4779–4786.

[63] T. Haneda, M. Kawano, T. Kojima, M. Fujita, *Angew. Chemie Int. Ed.* **2007**, *46*, 6643–6645.

[64] M. Zbačnik, B. Kaitner, *Croat. Chem. Acta* **2016**, *89*, 125–132.

[65] A. Carletta, J. Dubois, A. Tilborg, J. Wouters, *CrystEngComm* **2015**, *17*, 3509–3518.

[66] M. Zbačnik, B. Kaitner, *CrystEngComm* **2014**, *16*, 4162.

[67] B. C. Gates, H. Knözinger, F. C. Jentoft, *Advances in Catalysis Vol. 52*, Academic Press, **2009**.

[68] H. Ishida, S. Tobita, Y. Hasegawa, R. Katoh, K. Nozaki, *Coord. Chem. Rev.* **2010**, *254*, 2449–2458.

[69] L. J. Farrugia, *J. Appl. Cryst.* **2012**, *45*, 849–854.

[70] M. C. Burla, R. Caliandro, B. Carrozzini, G. L. Cascarano, C. Cuocci, C. Giacovazzo, M. Mallamo, A. Mazzone, G. Polidori, *J.*

Appl. Cryst. **2015**, *48*, 306–309.

[71] G. M. Sheldrick, *Acta Crystallogr. Sect. C, Struct. Chem.* **2015**, *71*, 3.

[72] A. L. Spek, *J. Appl. Cryst.* **2003**, *36*, 7–13.

[73] C. F. Macrae, P. R. Edgington, P. McCabe, E. Pidcock, G. P. Shields, R. Taylor, M. Towler, J. van de Streek, *J. Appl. Cryst* **2006**, *39*, 453–457.

[74] F. H. Allen, *Acta Crystallogr. Sect. B-Struct. Sci.* **2002**, *58*, 380–388.

Entry for the Table of Contents (Please choose one layout)

Layout 1:

FULL PAPER

Text for Table of Contents

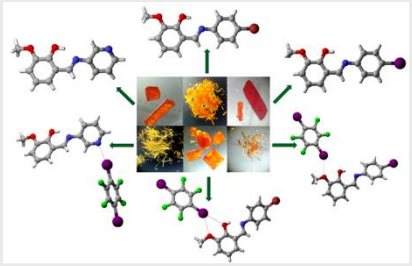

*Author(s), Corresponding Author(s)**

Page No. – Page No.

Title

Layout 2:

FULL PAPER

*Author(s), Corresponding Author(s)**

Page No. – Page No.

Title

Text for Table of Contents